# Expectations for $^{12}$C and $^{16}$O induced fusion cross sections at energies of astrophysical interest

C. L. Jiang, K. E. Rehm, B. B. Back, and R. V. F. Janssens
*Physics Division, Argonne National Laboratory, Argonne, Illinois 60439, USA*
(Received 6 October 2006; published 12 January 2007)

The extrapolations of cross sections for fusion reactions involving $^{12}$C and $^{16}$O nuclei down to energies relevant for explosive stellar burning have been reexamined. Based on a systematic study of fusion in heavier systems, it is expected that a suppression of the fusion process will also be present in these light heavy-ion systems at extreme sub-barrier energies due to the saturation properties of nuclear matter. Previous phenomenological extrapolations of the $S$ factor for light heavy-ion fusion based on optical model calculations may therefore have overestimated the corresponding reaction rates. A new "recipe" is proposed to extrapolate $S$ factors for light heavy-ion reactions to low energies taking the hindrance behavior into account. It is based on a fit to the logarithmic derivative of the experimental cross section which is much less sensitive to overall normalization discrepancies between different data sets than other approaches. This method, therefore, represents a significant improvement over other extrapolations. The impact on the astrophysical reaction rates is discussed.

DOI: 10.1103/PhysRevC.75.015803 PACS number(s): 26.50.+x, 25.60.Pj, 25.70.−z, 26.30.+k

## I. INTRODUCTION

Fusion reactions between nuclei such as $^{12}$C and $^{16}$O play an important role in the history of stellar evolution, especially in the interior of highly developed stars, where these reactions are important routes for the production of heavier elements. Because of their importance in nuclear astrophysics, many studies of these fusion reactions have been performed in the past. Although these processes occur at high temperatures in explosive scenarios, the Gamow energies are still very low, resulting in extremely small cross sections, which in many cases are not yet experimentally accessible [1–4]. In order to obtain the astrophysical reaction rates one has, therefore, to rely on phenomenological extrapolation methods. To facilitate these extrapolations, the concept of the $S$ factor ($S = \sigma E e^{2\pi\eta}$, where $\eta$ is the Sommerfeld parameter) has been introduced [1,5], which summarizes nuclear structure effects beyond standard barrier tunneling through a point-charge Coulomb barrier in a simple slowly-varying function. While this concept has been quite successful for reactions involving light projectiles such as hydrogen or helium, the higher Coulomb barriers and angular momenta, involved in the fusion reactions of heavier nuclei, result in strong energy dependences of the $S$ factor.

Some $S$ factors for light heavy-ion fusion reactions are plotted in Fig. 1 for systems ranging from $^{10}$B+$^{12}$C [6] to $^{16}$O+$^{16}$O [13–16]. The solid curves in Fig. 1 are optical model calculations which are used for extrapolating the $S$ factors toward lower energies. A similar figure was published in Ref. [6], but Fig. 1 includes some newer data. Although there is not always a good agreement among the various data sets, it is clear that the optical model predicts $S$ factors which are evidently larger than observed from the trend of the experimental data at the lowest energies. The optical model calculations show a continuous increase of $S(E)$, while many systems (e.g., $^{16}$O+$^{16}$O and $^{12}$C+$^{13}$C) point towards a decreasing $S(E)$ curve at the lowest energies. Such a maximum of the $S$ factor has been recently observed in medium heavy systems, where it was interpreted as a new fusion hindrance effect occurring at extreme sub-barrier energies [17–22]. In this paper, we discuss the effect of the fusion hindrance (a $S$ factor maximum) for lighter systems, using the systematics obtained from fusion reactions of both heavier and lighter nuclei as a guide [23]. This effect will introduce an important change both in the reaction mechanism and in the extrapolated $S$ factor and, consequently, also in the calculated astrophysical reaction rates.

In Sec. II, we present a brief description of the fusion hindrance in heavier systems and extend these results to the fusion of light heavy-ion reactions. A new recipe, an analytic formula for the excitation functions at very low energies is introduced in Sec. III. Based on these general results, we discuss in more detail the three reactions: $^{12}$C+C, $^{12}$O+$^{16}$O and $^{16}$O+$^{16}$O, which are important in stellar carbon and oxygen burning. The calculations of reaction rates and the comparisons with previous results for these three systems are presented in Sec. V followed by a short discussion and conclusion.

## II. HINDRANCE BEHAVIOR IN SYSTEMS FROM $Q < 0$ TO $Q > 0$

Fusion hindrance was first observed at extreme sub-barrier energies for five medium mass systems [17], and has since been confirmed for many other heavy-ion systems [18–22]. A good way to characterize the hindrance phenomenon is in terms of the energy $E_s$ where the $S$ factor for fusion develops a maximum [18]. It was first pointed out in Ref. [18] that, for heavy-ion fusion reactions with negative fusion $Q$-values, the $S$ factor must develop a maximum at low energies. For these systems the fusion cross section, $\sigma(E)$, must go to zero at the positive center-of-mass energy $E = -Q$, leading to the following asymptotic behavior,

$$\sigma(E) \to 0, \quad S(E) \to 0, \quad \text{for } E \to -Q, \quad \text{when } Q < 0, \tag{1}$$

 

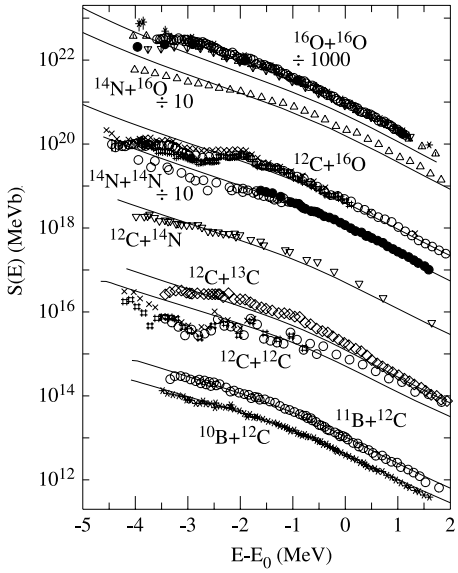


FIG. 1. Plot of $S(E)$ vs. $E - E_0$ ($E$ and $E_0$ are values of the center-of-mass energy and Coulomb barrier, respectively) for light heavy-ion fusion reactions $^{10}$B+$^{12}$C [6], $^{11}$B+$^{12}$C [6], $^{12}$C+$^{12}$C [7–9], $^{12}$C+$^{13}$C [6], $^{12}$C+$^{14}$N [6], $^{14}$N+$^{14}$N [6], $^{12}$C+$^{16}$O [10–12], $^{14}$N+$^{16}$O [6], and $^{16}$O+$^{16}$O [13–16]. Values of $E_0$ are 5.72, 5.63, 6.66, 6.57, 7.57, 8.61, 8.45, 9.62, and 10.76 MeV, respectively. The $Q$-values for these systems range from 32 to 15 MeV. The solid curves are optical model calculations with potential parameters $V = 50$ MeV, $W = 10$ MeV, $r_0 = 1.27$ fm and $a_0 = 0.40$ fm.

which results in a maximum of the $S$ factor at an energy $E_s > -Q$.

At energies below $E_s$ the fusion cross section $\sigma(E)$ therefore falls off steeply with decreasing energy $E$, much faster than predicted by present models, such as coupled-channels calculations using a Woods-Saxon potential. Surprisingly, this onset of fusion hindrance occurs at energies $E_s$ which correspond to relatively high excitation energies in the compound system; typically $E_{ex} \sim 20$–$40$ MeV.

Another way to discuss fusion hindrance is through the use of the logarithmic derivative of the energy weighted cross sections $L(E) = d[\ln(E\sigma)]/dE$ which shows a strong increase around $E_s$. From its definition, the logarithmic derivative is independent of a multiplicative factor in the cross sections. For the analysis of different experiments it, therefore, has the advantage that data, which differ by a constant factor (e.g., by using different detection efficiencies), produce the same $L(E)$, whereas the $S$ factors will be different. In the following discussion both representations will be used.

Present fusion models predict logarithmic derivatives that reach a constant value at low energies, or increase slowly with decreasing energy (see, e.g., the conventional coupled-channels calculations using a Woods-Saxon potential [24–26], which are shown in Figs. 2(a) and 2(b)), whereas the experimental data for $L(E)$ exhibit a strong, almost linear increase with decreasing energy around $E = E_s$ [17–22]. Again, this behavior of $L(E)$ can be understood from the definition of the logarithmic derivative, since

$$L(E) \to \infty, \quad \text{for} \quad E \to -Q, \quad \text{when} \quad Q < 0. \tag{2}$$

For comparison, we also introduce the logarithmic derivative expected from an excitation function for a point-like Coulomb potential at $l = 0$ [18,27]:

$$L_{cs}(E) = \frac{\pi\eta(E)}{E}, \tag{3}$$

where $\eta(E) = Z_1 Z_2 e^2/(\hbar v)$ is the Sommerfeld parameter. This quantity is also known as the "constant $S$ factor function," since the corresponding $S(E)$ curve is constant. As can be seen from Eq. (3) $L_{cs}(E)$ reaches a finite value at $E = -Q$. In Ref. [18] it was shown that the maximum of the $S$ factor coincides with the crossover energy of $L(E)$ and $L_{cs}(E)$.

In a recent publication, an explanation of the hindrance phenomenon for medium mass systems was presented [29]. In this model, the steep fall-off of the fusion cross section is related to the saturation properties of nuclear matter, which inhibit the large overlap of the reaction partners. This effect increases the repulsive part of the nuclear potential inside the barrier, resulting in a hindrance of quantum tunneling. This saturation property should also exist for lighter systems. It should be noted that in the early 1970's, Michaud indicated that, in order to reproduce the experimental cross sections of the three reactions $^{12}$C+$^{12}$C, $^{12}$C+$^{16}$O and $^{16}$O+$^{16}$O with an optical model, a (soft) repulsive core had to be artificially introduced [30]. The reason for adding a repulsive potential, however, was not recognized at that time.

Four examples of logarithmic derivatives and $S$ factors for the systems $^{64}$Ni+$^{64}$Ni ($Q = -48.8$ MeV), $^{58}$Ni+Ni ($Q = -66.1$ MeV), $^{12}$C+$^{13}$C ($Q = 16.3$ MeV) and $^{12}$C+$^{11}$B ($Q = 18.1$ MeV) are given in Figs. 2(a)–2(f). The two light systems were selected because contributions from resonances are small for these cases. The characteristics of the hindrance behavior for negative $Q$-value systems can be easily observed in Figs. 2(a) and 2(b). The experimental derivatives for the systems $^{64}$Ni+$^{64}$Ni and $^{58}$Ni+$^{58}$Ni cross the dashed line (expected for a point-like Coulomb potential) at energies $E_s = 87.4$ and 94.1 MeV (see Fig. 2(a)), which are also the energy locations of the corresponding $S$ factor maxima (see Fig. 2(b)). At these energies, the excitation energies in the compound systems are about 39 and 28 MeV.

For the lighter systems $^{12}$C+$^{13}$C and $^{11}$B+$^{12}$C the cross sections have not been measured to sufficiently low energies. Thus only approximate values for the crossing points of $L(E)$ and $L_{cs(E)}$ can be obtained (Figs. 2(c) and 2(e)). In the $S$ factor representation (Figs. 2(d) and 2(f)), broad maxima in $S(E)$ are observed. The maxima correspond to excitation energies of the compound nuclei of about 20 MeV, i.e., comparable to the values observed for the heavier systems mentioned above. The dot-dashed curves in Figs. 2(c)–2(f) are the logarithmic derivatives and $S$ factors, obtained from an optical model analysis, using the potential parameters from Stokstadt *et al.* ($V = 50$ MeV, $W = 10$ MeV, $r_0 = 1.27$ fm and $a = 0.4$ fm) [6]. At the lowest energies, the optical model overpredicts the $S$ factor and gives smaller values for the logarithmic derivative. At the higher energies, however, the optical model is in good agreement with the data.

An analysis of the heavier systems requires a full coupled-channels (CC) description, as shown by the dot-dashes curves in Figs. 2(a) and 2(b). Again, the conventional CC calculations

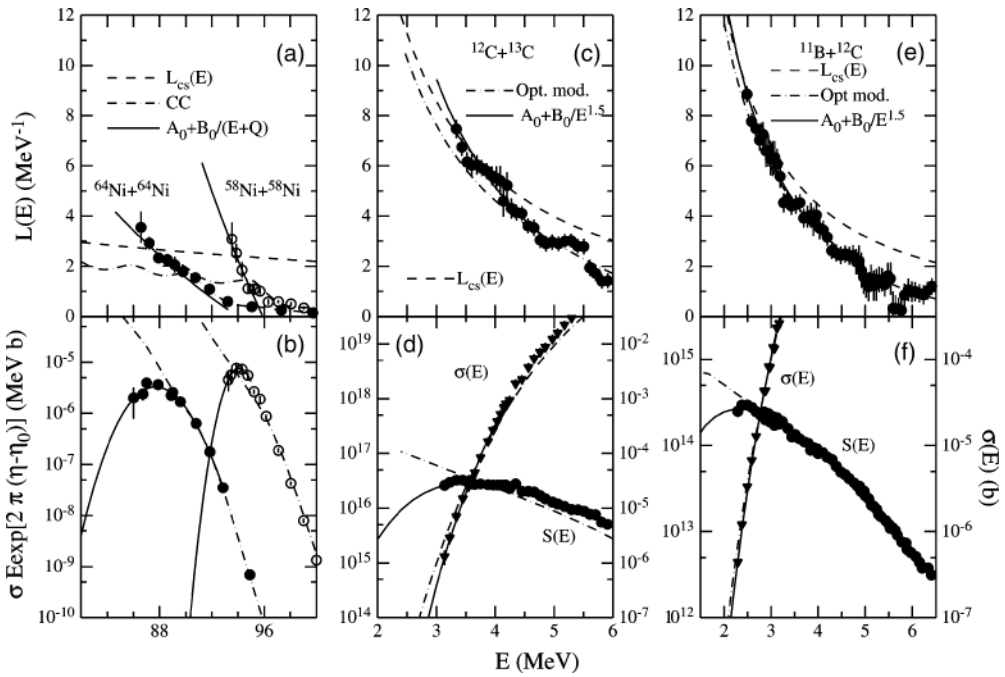


FIG. 2. (a) and (b) The fusion reactions $^{64}$Ni+$^{64}$Ni and $^{58}$Ni+$^{58}$Ni with data taken from Ref. [19] and [28], respectively. (a) Plot of $L(E)$ vs. $E$. The solid and open circles are the logarithmic derivatives obtained from least-squares fits to three experimental data points. The dashed curve is the constant $S$ factor result for the reaction $^{64}$Ni+$^{64}$Ni. The constant $S$ factor for the reaction $^{58}$Ni+$^{58}$Ni is almost identical. The solid lines are obtained from fits with the formula $A_0+B_0/(E+Q)$. The dot-dashed curves are from conventional coupled-channels calculations. (b) Corresponding plots of $S(E)$ vs. $E$. The solid curves in (b) are extrapolations, corresponding to the solid curves in (a). (c) and (d) The fusion reaction $^{12}$C+$^{13}$C with data taken from Ref. [6]. (c) Plot of $L(E)$ vs. $E$. The solid points are the logarithmic derivatives obtained from least-squares fits to five experimental data points, because the energy difference between the neighbouring data points is rather small. (d) Corresponding plots of $\sigma(E)$ vs. $E$ and $S(E)$ vs. $E$. The black triangles in (d) are the fusion cross sections with the scale given at the right side of the figure. The curves are identical to the ones in (a) and (b), but the fit was performed with the equation $A_0+B_0/E^{3/2}$ and the dot-dashed curves are the optical model calculations. (e) and (f) The fusion reaction $^{11}$B+$^{12}$C with data taken from Ref. [6]. The data points and the curves have the same definitions as in (c) and (d).

overpredict the $S$ factors at very low energies (see Refs. [17–22] for details).

Comparing the logarithmic derivatives for the light and the heavy systems in Figs. 2(a), 2(c), and 2(e), one observes a large difference in the pattern at which the experimental logarithmic derivative intersects the line $L_{cs}(E)$ expected from a point-charge Coulomb potential (dashed curve). For light heavy-ion fusion reactions (where the fusion $Q$-values are often positive), the curves $L(E)$ and $L_{cs}(E)$ are nearly parallel. Correspondingly, the $S$ factor maxima in these systems are sometimes difficult to recognize in a plot of $S(E)$ vs. $E$ alone. For the heavier systems $^{64}$Ni+$^{64}$Ni and $^{58}$Ni+$^{58}$Ni, the maximum in the $S$ factor is more easily visible.

The systematics of $L_s$ and $E_s$ as a function of the parameter $\zeta = Z_1 Z_2 \sqrt{\mu}$ has already been discussed in Refs. [18,23].

In principle, there does not have to be an intersection between the experimental logarithmic derivative $L(E)$ and $L_{cs}(E)$ for fusion reactions with positive $Q$-values, because the $S$ factor does not necessarily reach zero at $E = 0$. However, as discussed in Ref. [23], heavy-ion fusion hindrance may occur also for lighter systems with positive $Q$-values, down to $^{10}$B+$^{10}$B. This observation is consistent with the expectation that the saturation properties of nuclear matter should be included in the fusion mechanism for light heavy-ion reactions. For even lighter systems, the cross sections have not been measured to sufficiently low energies to draw any conclusion. The occurrence of the hindrance behavior depends on whether $L(E)$ grows faster than $L_{cs}(E)$ with decreasing energy, such that the two curves intersect. New measurements for these systems are needed. These experiments are, however, very difficult, since the cross sections are extremely small.

Another parametrization of $\sigma(E)$ which has sometimes been used for the systems $^{12}$C+$^{12}$C, $^{12}$C+$^{16}$O and $^{16}$C+$^{16}$O is given by

$$\tilde{S}(E) = \sigma E \exp(2\pi\eta + gE). \tag{4}$$

This representation compensates to a large extent for the remaining strong energy dependence of the traditional $S$ factor (see, e.g., Fig. 1). For the three reactions $^{12}$C+$^{12}$C, $^{12}$C+$^{16}$O, and $^{16}$O+$^{16}$O which are discussed below, both $S(E)$ and $\tilde{S}(E)$ representations will be used. The factor $g$ in Eq. (4) is given by [31]

$$g = \frac{2\sqrt{2}}{3\hbar}\left(\frac{\mu R^3}{Z_1 Z_2 e^2}\right)^{1/2}. \tag{5}$$

For the radii, $R$, we have used the values from Refs. [1,34]. The general structure of the energy dependence of the $S$ factor,

in particular the existence of a maximum, is not affected. The maximum in $\tilde{S}$ occurs at slightly higher energies than has been observed for the traditional $S$ factor, since the corresponding logarithmic derivative $L_{c\tilde{s}}(E)$ of constant $\tilde{S}$ factor is smaller than $L_{cs}(E)$ by $g$, i.e.,

$$L_{c\tilde{s}}(E) = L_{cs}(E) - g. \quad (6)$$

Thus $L_{c\tilde{s}}(E)$ intersects with $L(E)$ at an energy higher than $E_s$. The optical model calculations in the $\tilde{S}$ factor representation are again increasing continuously when the energy decreases and cannot reproduce a $\tilde{S}$ factor maximum either.

## III. POWER LAW EXTRAPOLATION FOR $Q > 0$ SYSTEMS

For reactions with positive $Q$-values, the following boundary conditions are expected for $E \to 0$:

$$\sigma(E) \to \text{finite } (\geqslant 0), \quad S(E) \to \text{finite or } \infty, \quad (7)$$

and

$$L(E) \to \infty, L_{cs}(E) \to \infty. \quad (8)$$

As shown in Figs. 1 and 2(c)–2(f), optical model calculations cannot reproduce the experimental data at very low energies because the hindrance behavior is not included in these calculations. On the other hand, a full understanding of the reasons behind the hindrance of sub-barrier fusion, especially for light heavy-ion systems, has not yet been achieved either. One, therefore, has to rely on phenomenology to extrapolate $\sigma(E)$ and $S(E)$ towards lower energies.

Because

$$L(E) = \frac{1}{E} + \frac{1}{\sigma}\frac{d\sigma}{dE}, \quad (9)$$

$L(E)$ reaches infinity with a rate equal to or faster than $1/E$. Since $L_{cs}(E) \propto 1/E^{3/2}$, which is the calculated logarithmic derivative for a point charge in the Coulomb penetration model, we fit the experimental $L(E)$ data for these light heavy-ion fusion reactions with an exponent $n = 3/2$ using the expression

$$L(E) = A_0 + B_0/E^n. \quad (10)$$

This expression fulfills the boundary conditions outlined in Eqs. (7) and (8). It should be noted that, for $n < 3/2$, $L(E)$ will intersect $L_{cs}(E)$ twice. In this case, after the maximum, with decreasing energy the $S$ factor will at first decrease, reach a minimum followed by an increase at even lower energies. The $S$ factor predicted in Ref. [32] shows a behavior just like the one mentioned above for $n < 3/2$.

With the parametrization given in Eq. (10) the cross section can be written as

$$\sigma(E) = \sigma_s \frac{E_s}{E} e^{\left[A_0(E-E_s) - B_0 \frac{1}{E_s^{n-1}(n-1)}\left[\left(\frac{E_s}{E}\right)^{n-1} - 1\right]\right]}, \quad (11)$$

with $n = 3/2$. The results of fitting the data for the systems $^{12}C+^{13}C$ and $^{11}B+^{12}C$ with Eq. (10) are displayed in Figs. 2(c) and 2(e) for $L(E)$ by the solid lines, and the corresponding $\sigma(E)$ and $S(E)$ are given in Figs. 2(d) and 2(f). The parameters $A_0$, $B_0$, $L_s$ and $\sigma_s$ are summarized in Table I.

A more elaborate parametrization of the $S$ factor, used for extrapolation purposes, has been suggested by Fowler *et al.* in Ref. [2]. It uses an analytically integrable form for the $S(E)$ factor based on the analysis of the reactions $^{12}C+^{12}C$, $^{12}C+^{16}O$ and $^{16}O+^{16}O$:

$$S(E) = S(0)\frac{\exp(-\alpha E)}{\exp(-\gamma E^m) + b\exp(+\beta E)}, \quad (12)$$

where $S(0), \alpha, \beta, \gamma, b$ and $m$ are fit parameters. This parametrization was chosen because of its similarity to optical model calculations for the reactions $^{12}C+^{12}C$, $^{12}C+^{16}O$ and $^{16}O+^{16}O$. Later, Ulke *et al.* [14] fitted their newly measured $^{16}O+^{16}O$ data with the same function.

Gasques *et al.* [4] have recently published an analytical expression of $S(E)$ for the fusion reaction $^{12}C+^{12}C$, covering a wide energy range:

$$S(E) = 5.15 \times 10^{16} \exp\left(-0.428E - \frac{3E^{0.308}}{1 + e^{0.613(8-E)}}\right), \quad (13)$$

which will also be discussed in the following sections.

The power law extrapolation discussed above has been developed for systems with positive $Q$-values. The procedure can easily be extended to negative $Q$-value systems, and the solid lines for the systems $^{64}Ni+^{64}Ni$ and $^{58}Ni+^{58}Ni$, shown in Figs. 2(a) and 2(b), are obtained from those extrapolations. They will not be discussed further in the present paper.

TABLE I. Results obtained from least-squares fits to the low-energy data with Eqs. (10) and (11) and $n = 3/2$ for fusion reactions with positive $Q$-values. $E_s$ and $L_s$ are the values of the energy and the logarithmic derivative where $S(E)$ has a maximum. $A_0$ and $B_0$ are obtained from least-squares fits with Eq. (10), and $N$ is the number of data points used in the fit. $\sigma_s$ is the value of the fitted cross section at the maximum of the $S$ factor with $A_0$, $B_0$, $E_s$ and Eq. (11); values in the parentheses correspond to the highest or lowest results obtained in the fits using only cross sections from one experiment. The fusion $Q$-values and factors $\zeta = Z_1 Z_2 \sqrt{\mu}$ are included for reference.

| System | $n$ | $E_s$ MeV | $L_s$ MeV$^{-1}$ | $N$ | $A_0$ MeV$^{-1}$ | $B_0$ MeV$^{1/2}$ | $\sigma_s$ mb | $Q$ MeV | $\zeta$ | Ref. |
|---|---|---|---|---|---|---|---|---|---|---|
| $^{11}B+^{12}C$ | 1.5 | 2.12 | 11.5 | 40 | −1.81 | 41.17 | $9.3 \times 10^{-5}$ | 18.198 | 71.9 | [6] |
| $^{12}C+^{13}C$ | 1.5 | 3.45 | 6.94 | 53 | −2.32 | 59.37 | $1.5 \times 10^{-2}$ | 16.318 | 89.9 | [6] |
| $^{12}C+^{12}C$ | 1.5 | 3.68 | 6.18 | 69 | −1.32 | 52.93 | $2.3(+0.4,-0.3)\times10^{-2}$ | 13.934 | 88.2 | [7–9] |
| $^{12}C+^{16}O$ | 1.5 | 4.54 | 6.43 | 151 | −2.01 | 82.35 | $1.1(+0.1,-0.3)\times10^{-3}$ | 16.756 | 125.7 | [10–12] |
| $^{16}O+^{16}O$ | 1.5 | 6.78 | 5.07 | 50 | −4.11 | 162.0 | $8.0(+1.7,-3.0)\times10^{-3}$ | 16.542 | 181.0 | [13–16] |

## IV. THE FUSION REACTIONS $^{12}$C+$^{12}$C, $^{12}$C+$^{16}$O AND $^{16}$O+$^{16}$O

We will now discuss the results from different extrapolation methods for the three fusion reactions involving $^{12}$C and $^{16}$O nuclei. Many measurements of these three reactions, which are important during the astrophysical carbon and oxygen burning phases, have been performed in the past [7–16,33–44]. Large discrepancies between different measurements complicate the extrapolations, as discussed in more detail below. In addition, the parametrization developed above was derived from an analysis of structureless excitation functions. For some lighter nuclei, especially for the system $^{12}$C+$^{12}$C, strong resonances in the excitation functions are observed. In this case, one has to keep in mind that the present parametrization cannot describe the complete structure of the excitation function, but can only reproduce its energy-averaged behavior. Because the extrapolations are used mainly in calculations of astrophysical reaction rates, the detailed structure is washed out by the integration and thus, only the average behavior of the excitation function is important. The other extrapolations proposed in the literature do not consider contributions from the resonances either, and thus also provide a description of the energy-averaged excitation function only. In the following, the three systems will be discussed individually, concentrating mainly on data measured at the lowest energies [7–16].

### A. $^{16}$O+$^{16}$O

As can be seen from Fig. 1, this system is least influenced by low-energy resonances. However, there are large discrepancies among the different experiments which are partly due to difficulties with the $^{16}$O targets used in the experiments. There are four independent absolute total cross section measurements for the $^{16}$O+$^{16}$O fusion reaction covering the low-energy region [13–16]. In addition, Spinka *et al.* [13], also measured a relative excitation function over a wider energy range, normalized to their own absolute cross section at $E = 9.85$ MeV. These five experimental data sets are plotted as the logarithmic derivative $L(E)$, as the $S$ factor $S(E)$ and as $\tilde{S}(E)$ in Fig. 3. At the lowest energies, the various data differ by up to a factor of five. The predictions of the different models are represented by the various lines in Fig. 3. The optical model calculation (black solid line) is in poor agreement with the data, especially in the $S$ factor representation. Fits to the data of Spinka *et al.* [13] or of Hulke *et al.* [14] using the parametrization of Fowler [Eq. (12)] are shown by the black dot-dashed and light-blue dashed curves, respectively. The fit parameters for $S(0), \alpha, \beta, \gamma, b$ and $m$ are $1.24 \times 10^{27}, 0.78, 0.681, 9.06 \times 10^{-6}, 3.89 \times 10^{-4}, 6$, and $1.24 \times 10^{28}, 0.72, 0.68, 9.80 \times 10^{-6}, 4.37 \times 10^{-3}$ and 6, respectively. The agreement with the majority of the experimental data in the critical energy region around $E \sim 7$–8 MeV, however, is not good. In order to emphasize the differences between the various experiments, especially at the lowest energies, these data sets have been plotted separately in Fig. 4. Analyzing each data set separately, one observes that the majority of the data show a maximum in the $S$ factor, as indicated by the dashed lines in Fig. 4. The maximum in the $S$ factors, however, does not occur at the same energy in different data sets. Since most experimental data for $S(E)$ exhibit a maximum, the description of the $S$ factor for $^{16}$O+$^{16}$O by Eq. (12) which is continuously increasing at low energies, is not justified.

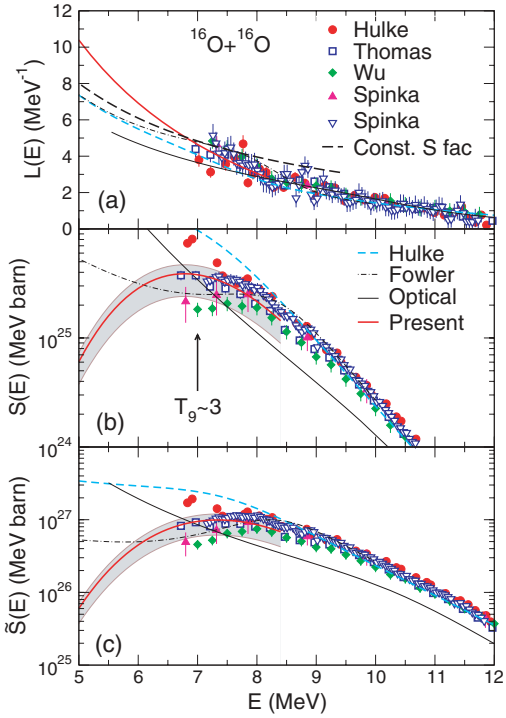


FIG. 3. (Color) (a) Plot of $L(E)$ vs. $E$ for the fusion of $^{16}$O+$^{16}$O. The derivatives were obtained by least-squares fits to three cross section points. The black long-dashed curve corresponds to a constant $S$ factor. (b) Plot of $S(E)$ vs. $E$ and (c) Plot of $\tilde{S}(E)$ vs. $E$ for the same reaction of $^{16}$O+$^{16}$O; the symbols and curves are the same in (a), (b), and (c). The black solid curve is from optical model calculations, and the light-blue dashed and black dot-dashed curves are the extrapolations obtained by Hulke *et al.* [14] and by Fowler *et al.* [2], respectively. The red solid line is the extrapolation obtained in the present paper. See text for details.

The logarithmic derivative is, as mentioned above, insensitive to scaling factors and depends only on the slope of the excitation function. The corresponding plot of $L(E)$ vs. $E$ is shown in Fig. 3(a). Although the data still scatter substantially, the relative deviations are considerably smaller than in the $S(E)$ vs. $E$ plot (Fig. 3(b)). On average, the shape of the function $L(E)$ is similar to the data shown in Figs. 2(c) and 2(e) for the systems $^{12}$C+$^{13}$C and $^{11}$B+$^{12}$C. The experimental $L(E)$ curve intersects with the point-charge $S$ factor curve $L_{cs}(E)$ at about 7 MeV and approaches the optical model curve (shown by the black solid line) at higher energies. Because of its smaller scatter, it is more appropriate to use the logarithmic derivative representation, $L(E)$, in a study of the asymptotic behavior and for extrapolation purposes. Altogether, there are 172 $L(E)$ data points from the five measurements for the fusion reaction $^{16}$O+$^{16}$O. Taking $n = 3/2$ and the 50 lowest energy data points (to be discussed later) for a fit using Eq. (10), one obtains the result shown by the red solid line in Fig. 3(a), with the parameters listed in Table I together with the values obtained for other systems. The corresponding curves for the

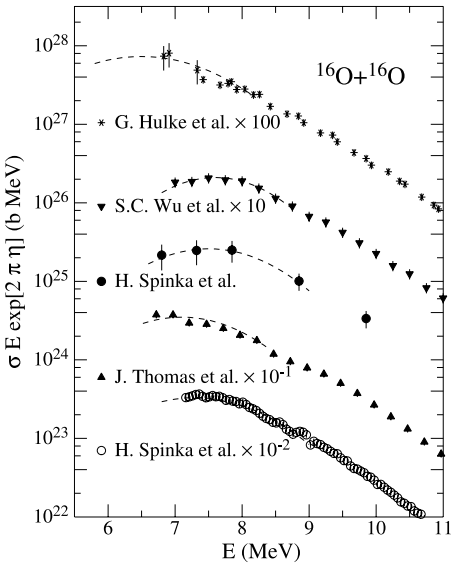


FIG. 4. $S$ factors for the fusion reaction $^{16}$O+$^{16}$O. Data from [13–16] are multiplied by different scaling factors as indicated in the plot. The dashed curves serve only to guide the eye.

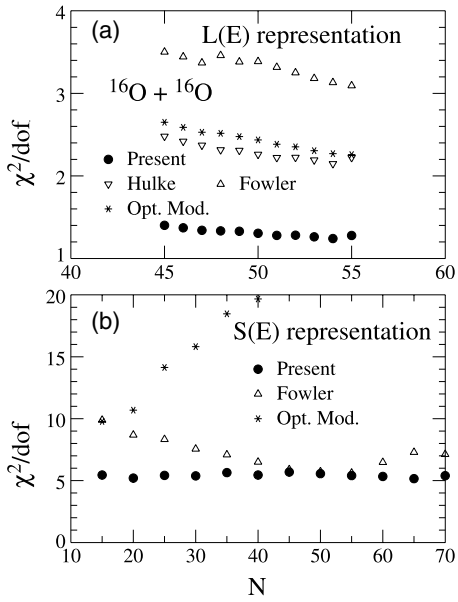


FIG. 5. Plots of $\chi^2$/dof vs. $N$ for the $L(E)$ representation (a) and the $S$ factor representation (b) for system $^{16}$O+$^{16}$O. The value $N$ is the number of experimental data points used in the calculations (starting with the lowest energy) and dof are the degrees-of-freedom. In (b), Hulke's results are not shown because they are off scale.

$S$ factor and $\tilde{S}(E)$ are shown by red solid lines in Figs. 3(b) and 3(c), respectively.

The logarithmic derivative of Fowler's analytic extrapolation Eq. (12) at extreme sub-barrier energies is given by

$$L_{\text{Fowler}}(E) = -\alpha + \frac{D_0}{E^{3/2}}. \tag{14}$$

Here $D_0 = 0.495 Z_1 Z_2 \sqrt{\mu}$ is the same parameter as in Eq. (3). The energy dependence $1/E^{1.5}$ is the same in both equations. This means that

$$L_{\text{Fowler}}(E) - L_{\text{cs}}(E) = -\alpha, \tag{15}$$

at very low energies. Values of $\alpha = 0.78$ and $\alpha = 0.72$ were obtained by Fowler and Hulke, respectively. Thus, $L_{\text{Fowler}}(E)$ [also $L_{\text{Hulke}}(E)$] will never intersect $L_{\text{cs}}(E)$ and increase at low energies parallel to $L_{\text{cs}}(E)$.

A quantitative comparison of these different fits is provided in Fig. 5. Here, the $\chi^2$ [defined as $\Sigma(\frac{Y_i - F_i}{\Delta Y_i})^2$] per degrees of freedom, $\chi^2$/dof, is plotted as a function of the number of experimental data points, $N$, included in the fit (starting from the lowest energy) to the $L(E)$ and $S$ factor representations, using three sets of fit functions: the present parametrization [Eqs. (10) and (11)], that of Fowler and Hulke [Eq. (12)], and the optical model. As can be seen in Fig. 5(a), if the number of $L(E)$ data points is within 50 to 55 (i.e., covering the energy range of 6.96 to 8.47–8.64 MeV), the resulting $\chi^2$/dof values are small and stable. This is the reason why 50 data points of $L(E)$ were used in our final fitting procedure. The $\chi^2$/dof obtained from Fowler's and Hulke's extrapolations or from optical model calculations are much worse. The $\chi^2$/dof vs. $N$ for the $S$ factor representation is presented in Fig. 5(b). Obviously, the $\chi^2$/dof is bigger for $S(E)$ than for $L(E)$, as was discussed above. In Fig. 5(b), Hulke's results are not shown because they are off scale.

The red solid $S(E)$ curve given in Fig. 3(b) corresponds to a $\sigma_s$ value, which is obtained with the parameters $A_0$, $B_0$, $E_s$ and Eq. (11) using data from all the experiments cited. The two $\sigma_s$ values in parentheses in Table I are obtained by using only Hulke's (experimentally highest [14]) or Wu's (experimentally lowest [15]) data, respectively. The band around the red curve shown in Fig. 3(b) is obtained with these two values.

Although the exact shape of $S(E)$ below $E < 7$ MeV cannot be predicted well, the shape of $S(E)$ observed in the majority of the experiments points towards fusion hindrance for the $^{16}$O+$^{16}$O system.

The general pattern in the $S(E)$ and $\tilde{S}(E)$ representations is rather similar (see Figs. 3(b) and 3(c)). The maximum in $\tilde{S}(E)$ is even more pronounced than the one in $S(E)$. The optical model calculations and the extrapolation of Hulke do not predict a $\tilde{S}$ factor maximum, while the present and Fowler's extrapolations do. The difference between the latter two becomes more pronounced when the energy decreases.

### B. $^{12}$C+$^{16}$O

The experimental data for the low-energy fusion of $^{12}$C+$^{16}$O [10–12] are given in Fig. 6. There is some evidence for resonances in this excitation function at low energies. The black solid curves are the result of optical model calculations. They agree with the data at higher energies, but overpredict the cross sections below ~6 MeV. The black dot-dashed curves are Fowler's extrapolations [Eq. (12)]. The parameters $S(0)$, $\alpha$, $\beta$, $\gamma$, $b$ and $m$ obtained by Fowler *et al.* for this system are $1.15 \times 10^{21}$, 0.643, 0.837, $6.26 \times 10^{-3}$, $1.6 \times 10^{-3}$ and 3, respectively. These curves for $S(E)$ and $L(E)$ agree better with the experimental data than the optical model calculations.

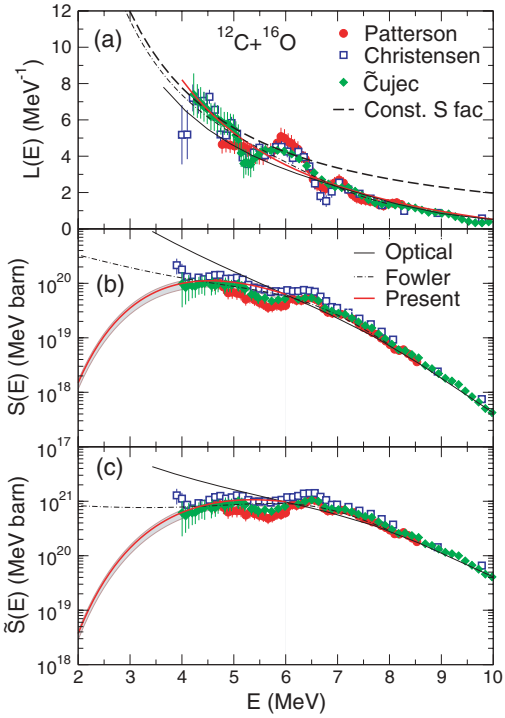


FIG. 6. (Color) Plot of (a) $L(E)$, (b) $S(E)$ and (c) $\tilde{S}(E)$ for the fusion reaction $^{12}$C+$^{16}$O with data taken from Refs. [10–12]. The derivatives were obtained by least-squares fits to eight, five, and five cross section points for Patterson's, Christensen's, and Čujec's experiments, respectively. The black long-dashed line corresponds to a constant $S$ factor, while the black solid line is the result of an optical model calculation. The black dot-dashed curves correspond to the fit obtained by Fowler *et al.* [2]. The red solid lines are the results of least-squares fits to the data using Eqs. (10) and (11). See text for details.

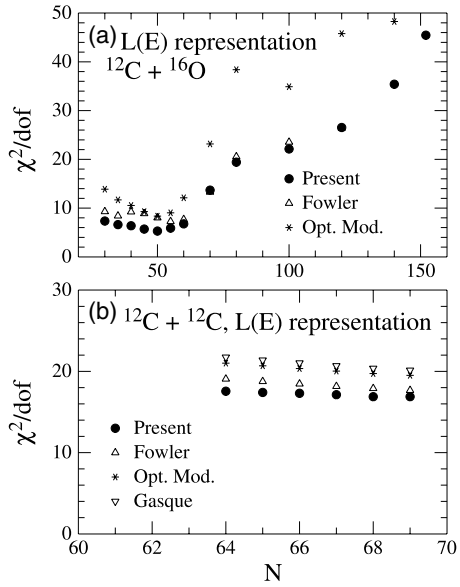


FIG. 7. Plots of $\chi^2$/dof vs. $N$ for the $L(E)$ representation, (a) $^{12}$C+$^{16}$O, (b) $^{12}$C+$^{12}$C. The value $N$ is the number of experimental data points used in the calculations (starting with the lowest energy). The symbol dof means degrees-of-freedom. Some data points are not shown because they are off scale.

Though not as obvious as in the case of $^{16}$O+$^{16}$O, there is evidence for a maximum of the $S$ factor in this reaction. A least-squares fit of all 151 experimental $L(E)$ data points (from the three excitation functions cited) with the function $A_0+B_0/E^{3/2}$ is given by the red solid curve in Fig. 6(a). This fit gives a good description of the data at the lowest energies. The corresponding extrapolation for $S(E)$ is shown by the red solid curve in Fig. 6(b), resulting in a good description of the experimental data. The fit parameters are listed in Table I.

A quantitative comparison of different fits for $^{12}$C+$^{16}$O is provided in Fig. 7(a), with a plot of $\chi^2$/dof as a function of $N$ for the $L(E)$ representation. Due to the resonances, which are not described by the extrapolation functions, the values of $\chi^2$/dof are higher than the ones for the $^{16}$O+$^{16}$O reaction. However, the present function is slightly better than previous fits. The important difference between these fits appears in the energy region lower than the measured data points. Although there is a minimum of $\chi^2$/dof for $N = 50$, corresponding to an energy range of ∼5 MeV and covering a wing of a resonance, we prefer to take the whole range, which includes an average of several resonances, i.e., all 151 data points.

The red solid $S(E)$ curve shown in Fig. 6 corresponds to the $\sigma_s$ value listed in the Table I, which is obtained from all, 167 cross section data points. The band around the red $S(E)$ curve corresponds to the values included in parentheses, which are obtained from fits to Christensen's [12] or Patterson's [10] experimental data only.

Similar to the case of $^{16}$O+$^{16}$O, the maximum is more pronounced in the $\tilde{S}$ factor representation, while the optical model calculation and Fowler's extrapolation do not predict a $\tilde{S}$ factor maximum.

### C. $^{12}$C+$^{12}$C

Because it has the lowest Coulomb barrier among the three reactions discussed in this section, and because of the relatively high $^{12}$C abundance in the universe, fusion between $^{12}$C+$^{12}$C is the most important heavy ion reaction in nuclear astrophysics. It has been studied in the past in numerous experiments, using both gamma and particle detection techniques. Experimental data [7–9] for energies below $E_{\text{c.m.}} \sim 9$ MeV are presented in Fig. 8. The fluctuations in the experimental cross sections are noticeable, especially in the $L(E)$ representation. A detailed comparison of the experimental data shows, however, that the cross sections obtained by the various groups differ considerably. In addition, resonances play a significant role even at the lowest energies measured so far for this reaction. Recently, new data for an excitation function in the energy range of 4.42–6.48 MeV [45] have been obtained using the $\gamma$-ray detection technique. In this experiment, the resonance peaks observed in the energy region have been used to correct the energy scales obtained in earlier measurements. The arguments for the introduction of these energy shifts are mainly based on carbon buildup on the target during the experiment. Since the amount of carbon buildup depends on the running time, it is not clear whether a constant energy shift should be chosen. Furthermore, at

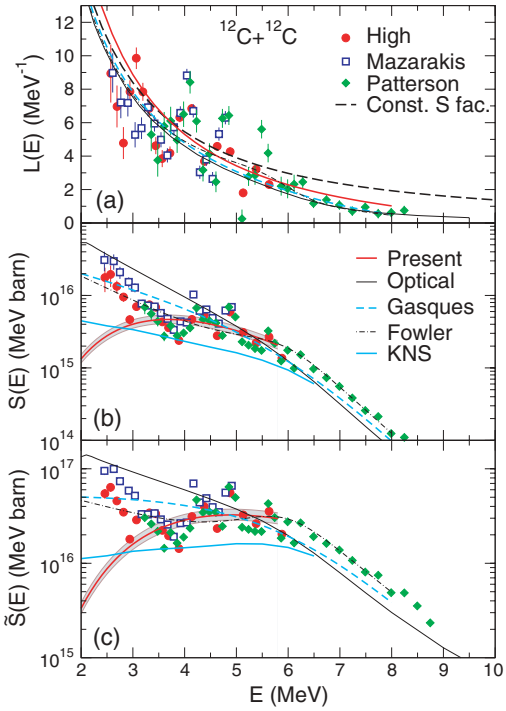


FIG. 8. (Color) $L(E)$, $S(E)$, and $\tilde{S}(E)$ vs. $E$ plots for the system $^{12}$C+$^{12}$C. The derivatives were obtained by least-squares fits to three cross section points. The symbols and curves are similar to those of Figs. 3 and 6. The light-blue solid curves shown in (b) and (c) are the calculations for the "nonresonant part" of $\tilde{S}(E)$ given in Ref. [45] with the Krappe-Nix-Sierk (KNS) nuclear potential [46].

the lowest energies ($E < 3$ MeV), the agreement does not improve with these corrections. Due to these uncertainties and since the present discussion is concentrated in the low-energy region, we have, therefore, decided not to use these corrections in our extrapolation procedure. Because of these complications and the lack of data below 3 MeV, it is obvious that an analysis of the data using Eq. (10), which describes only the average behavior of the cross sections, is difficult. New data at lower energies are urgently needed for this astrophysical important system.

A least-squares fit to all, 69 experimental $L(E)$ data in Fig. 8(a) using Eq. (10) is illustrated by the red solid line, which does intersect the constant $S$ factor curve at $E_s = 3.7$ MeV. The fit parameters are summarized in Table I.

The results from earlier extrapolations are represented by the various lines in Fig. 8. The optical model description shown by the black solid line again overestimates the cross sections at the lowest energies. In fact, this description results in values that exceed the cross section at the peak of the strong resonance. The extrapolation obtained by Gasques *et al.* [4] with Eq. (15) (light-blue dashed curve) gives a good description of the average of the data in the energy region where cross section measurements have been performed. A similar conclusion is reached with Fowler's extrapolation (black dot-dashed curves) using Eq. (12). The parameters obtained for $S(0), \alpha, \beta, \gamma, b$ and $m$ are $8.83 \times 10^{16}$, 0.772, 0.697, $5.01 \times 10^{-3}$, $5.56 \times 10^{-3}$ and 6, respectively.

A quantitative comparison of the $\chi^2$/dof as a function of $N$ for different fits to the logarithmic derivative for $^{12}$C+$^{12}$C is shown in Fig. 7(b). Similar to the $^{12}$C+$^{16}$O reaction, the presence of resonances prevents a small value of $\chi^2$/dof. Again, as compared to other extrapolations, the present one reduces the $\chi^2$/dof somewhat. Using all the $L(E)$ data points (i.e., $N = 69$) which cover a wide range in energy, the fit describes the average behavior satisfactorily. The red solid $S(E)$ curve provided in Fig. 8(b) corresponds to the $\sigma_s$ value listed in Table I (using all 75 data points). The band corresponds to the $\sigma_s$ values included in the parentheses. In a comparison of the experimental $S(E)$ data with the various extrapolations it should be noted that, as stated in Ref. [9], the $S$ factor at the lowest energies is dominated by a resonance. None of the extrapolation procedures discussed above include the contributions from resonances. As can be seen in Figs. 8(b) and 8(c), the extrapolations of Refs. [2,4] seem to follow the maxima of the resonances, while the extrapolation recipe developed in this paper represents the energy behavior of the nonresonant (direct) part of the cross section.

In Ref. [45], the data have been analyzed using the Krappe-Nix-Sierk (KNS) nuclear potential [46] to calculate the "nonresonant part" of $\tilde{S}(E)$. The result is given by the light-blue solid curves in Figs. 8(b) and 8(c). As shown in Ref. [45], this potential is broader than other potentials used in the analysis, leading to a reduction of the penetrability at lower energies. In this manner, it may include part of the contribution of the hindrance behavior. A broader $\tilde{S}(E)$ maximum appears in this calculation.

From this discussion it is clear that, for the $^{12}$C+$^{12}$C system, new measurements extending to energies below 3 MeV are needed in order to obtain better estimates for the cross section behavior at astrophysical energies.

## V. REACTION RATES FOR CARBON AND OXYGEN BURNING SYSTEMS

The astrophysical reaction rate is given by (see Ref. [1])

$$\langle \sigma v \rangle = \left(\frac{8}{\pi \mu}\right)^{1/2} \frac{1}{(kT_9)^{3/2}} \int \sigma E \exp\left(-\frac{E}{kT_9}\right) dE. \quad (16)$$

This expression depends strongly on the temperature $T_9$, through the Maxwellian factor $\exp(-\frac{E}{kT_9})$ in the integrant. Carbon burning in evolved massive stars takes place at densities of $\rho \sim 10^9$ g/cm$^3$ and temperatures of $\sim$(6–8) $\times$ $10^8$ K. In type Ia supernovae, the explosions are driven by carbon ignition in cores of accreting massive CO white dwarfs. The ignition conditions are typically around $T \sim (1.5 - 7) \times 10^8$ K [4]. In other explosive scenarios, temperatures as high as several $10^9$ K can occur [3]. Therefore, reaction rates are needed for a broad range of stellar temperatures. In all cases, experimental data at very low energies are unfortunately not available, which complicates the extrapolation and the calculation of the astrophysical reaction rate. Contrary to other extrapolations discussed above, the results obtained in this analysis include the effect of fusion hindrance. It should be noted that the reaction rates calculated from the bands around

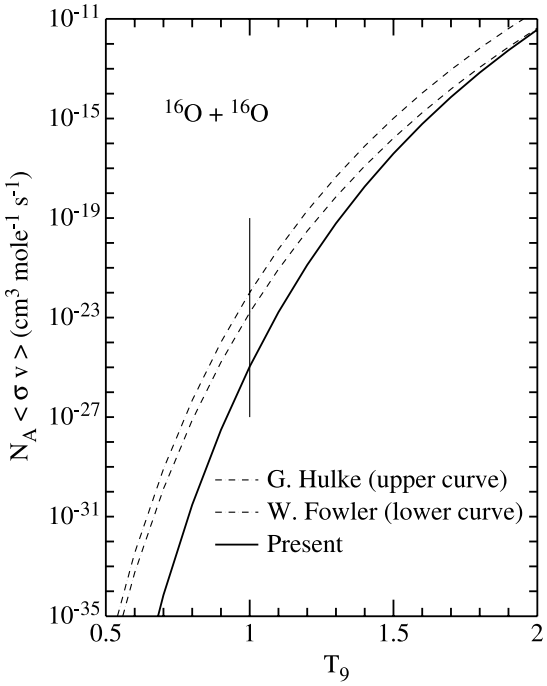


FIG. 9. Calculated reaction rates for the fusion reaction $^{16}$O+$^{16}$O. The upper and lower dot-dashed curves are obtained from Hulke's and Fowler's extrapolations, respectively. The solid curve is obtained with the present extrapolation.

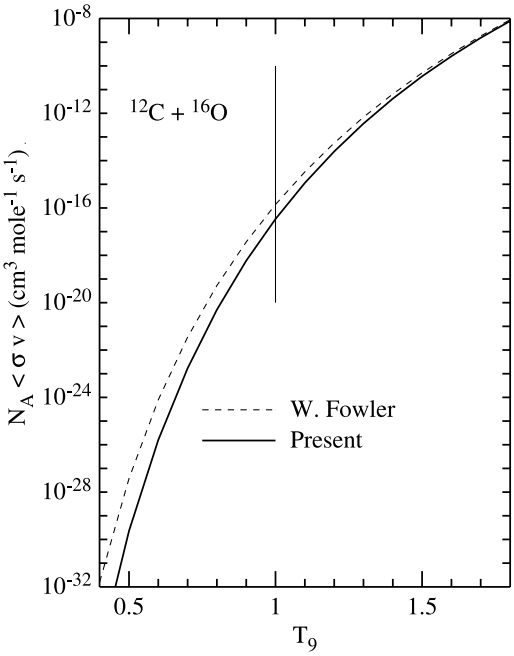


FIG. 10. Calculated reaction rates for the fusion reaction $^{12}$C+$^{16}$O. The dot-dashed and the solid curves are obtained from Fowler's and the present extrapolation, respectively.

the red $S(E)$ curves discussed above, fall within the width of the solid curves, shown in Figs. 9, 10, and 11.

For the fusion reaction $^{16}$O+$^{16}$O, a temperature of $T_9 = 3$ corresponds to an effective energy of ∼7 MeV (see Fig. 3(a)), which is about the energy of the lowest data point measured so far. Obviously, especially for lower stellar temperatures, the different extrapolations discussed in the previous section will give different results for the astrophysical reaction rates. The calculated reaction rates for three extrapolations are presented in Fig. 9, i.e., Hulke *et al.* (upper dot-dashed line, [14]), Fowler *et al.* (lower dot-dashed line, [2]) and the present analysis (solid line). Here the rate of Hulke *et al.* is higher than that of Fowler *et al.*, reflecting the fact that Hulke's $S(E)$ factor is always higher. The difference between the two rates is about a factor of 5 at lower temperatures, and decreases to a factor of 2 at higher temperatures. The results from the present extrapolation are much smaller than the other two, except at temperatures above $T_9 \sim 2$, which is obvious from the difference in the $S$ factors discussed above.

The reaction rates calculated for the fusion reaction $^{12}$C+$^{16}$O are presented by similar line styles in Fig. 10. The difference between the present result and the rate obtained by Fowler *et al.* [2] at $T_9 = 1$ is about a factor of 3–5. At lower stellar temperatures, the difference increases rapidly. At high temperatures ($T_9 \sim 2$), the two extrapolations give similar results, since the contributions to the reaction rate come from the energy region covered by experimental cross section measurements, where the influence of the extrapolated part of the cross sections is small.

The reaction rates calculated for $^{12}$C+$^{12}$C fusion are provided in Fig. 11. The results obtained by Fowler *et al.* [2] and Gasques *et al.* [4] are very similar. At higher temperatures, they agree well with the results obtained from the present extrapolation. From the discussion given in the previous section, it is possible that, at low energies, the present extrapolation may represent a lower limit of the reaction rates

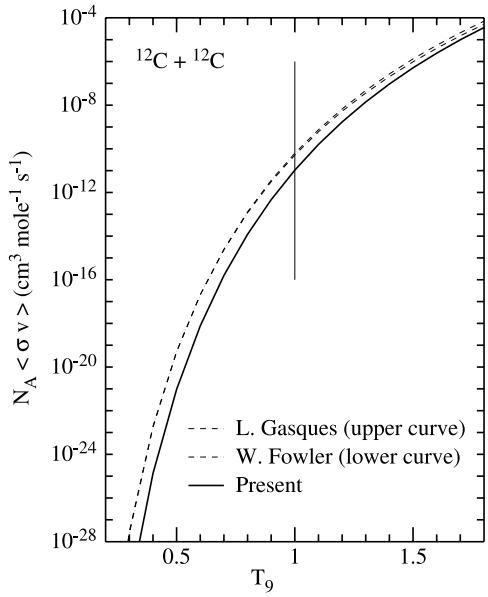


FIG. 11. Calculated reaction rates for the fusion reaction $^{12}$C+$^{12}$C. The dot-dashed curves are obtained from Gasques' and Fowler's extrapolations, respectively. These two extrapolations are very similar at low temperatures, and Gasques' extrapolation is slightly higher than Fowler's at high temperatures. The solid curve is obtained with the present extrapolation.

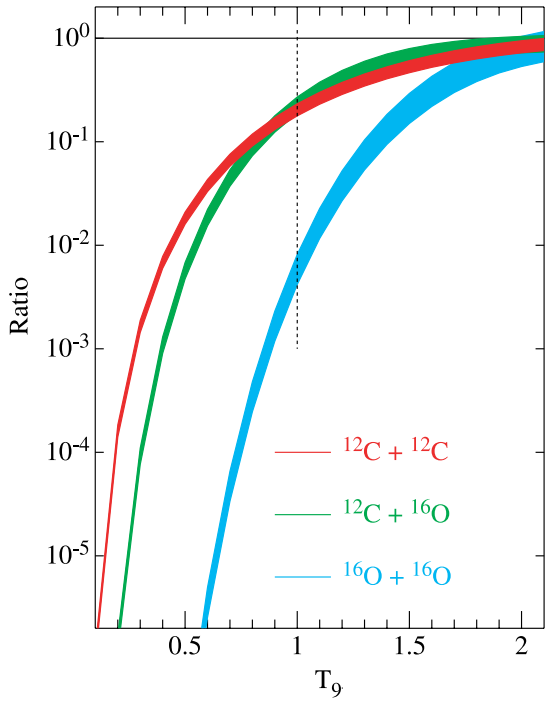


FIG. 12. (Color) Ratios of reaction rates for the three fusion reactions $^{12}C+^{12}C$ (red), $^{12}C+^{16}O$ (green) and $^{16}O+^{16}O$ (light-blue). These bands [made from the corresponding three $S(E)$ bands] are the ratios between the present extrapolation and that proposed by Fowler [2]. See text for details.

since contributions from resonances at the lowest energies are not included. On the other hand, it can be concluded that the extrapolations from Fowler *et al.* [2] and Gasques *et al.* [4] give a good description in the measured energy region, and might represent possible upper limits for the reaction rates at lower temperatures. The presence of low energy resonances, however, makes it difficult to predict precise values of the astrophysical reaction rates.

The ratios of reaction rates calculated from the present extrapolation to Fowler's compilation [2] for the three fusion reactions $^{12}C+^{12}C$, $^{12}C+^{16}O$ and $^{16}O+^{16}O$ are summarized in Fig. 12 as red, green and light-blue bands, respectively.

Obviously, the influence of fusion hindrance is more pronounced for the reaction $^{16}O+^{16}O$. At a temperature $T_9 \sim 1.0$ the ratios differ by factors of up to 100. For the reactions $^{12}C+^{16}O$ and $^{12}C+^{12}C$, the differences of the ratios are in the range 1.5–3 and 1–5, respectively. At lower temperatures, the differences increase rapidly.

## VI. DISCUSSION AND CONCLUSION

The concept that fusion hindrance at extreme sub-barrier energies occurs in all heavy-ion induced fusion reactions has been explored here for light systems of interest in astrophysics. Fusion hindrance influences both the reaction mechanism and the calculations of the astrophysical reaction rates. If the fusion hindrance is due to the saturation properties of nuclear matter (and the Pauli exclusion principle), it should also be present in light heavy-ion systems.

We have shown that optical model calculations for light heavy-ion fusion always overpredict the excitation functions at extreme low energies, where the fusion hindrance occurs. Based on the observation that the logarithmic derivative of the energy-weighted fusion cross section, $L(E)$, has a rather slow dependence at energies around the $S$ factor maximum, and by considering the asymptotic behavior of $L(E)$, we have suggested a simple analytic expression for this representation which can be used for extrapolating excitation functions of heavy-ion fusion reactions to lower energies.

None of the three systems has yet been measured to sufficiently low energies to determine whether a maximum in the $S$ factor occurs in these light systems. The $^{12}C+^{16}O$ system is perhaps experimentally the easiest for extending these measurements towards lower energies, since it requires a solid $^{12}C$ target and there is only a moderate resonant structure. The cross sections, however, are small (this system has been measured down to ~25 nb already) and, as seen from earlier experiments, the buildup of $^{12}C$ on the target needs to be carefully monitored.

Calculations of the reaction rates have been carried out for the important fusion reactions of carbon and oxygen burning: $^{12}C+^{12}C$, $^{12}C+^{16}O$ and $^{16}O+^{16}O$. The results show that the hindrance phenomenon can cause large differences (up to orders of magnitude) between the present rates and the values obtained in the past for temperatures $T_9 \leqslant 1$, i.e., for the temperature range important for reactions occurring in the late evolution of massive stars and in type-Ia supernova explosions.

A study of the influence of these reduced astrophysical reaction rates in various astrophysical scenarios depends on the details of the stellar environment and is beyond the scope of this paper. It will be interesting to determine whether the reduction in the rates caused by fusion hindrance can be compensated by appropriate changes in stellar conditions (such as ignition temperatures, densities, etc.).

Since the physical nature of fusion hindrance at extreme low energies is still a matter of debate, many questions need to be answered by future experiments and better theoretical treatments. The extrapolation method presented in this paper is only a first step which hopefully will trigger future fusion measurements as well as theoretical studies of these important light heavy-ion systems and improves our understanding of the reaction mechanism at extremely low energies.

## ACKNOWLEDGMENTS

The authors thank J. Truran, A. Heger, and H. Spinka for valuable discussions about the astrophysical results of the paper, and about the experimental data for the fusion reaction $^{16}O+^{16}O$. We would like also to thank H. Esbensen and Ş. Mişicu for numerous discussions about the nature of the fusion hindrance phenomenon. This work was supported by the U.S. Department of Energy, Office of Nuclear Physics, under Contract No. DE-AC02-06CH11357.

[1] C. E. Rolfs and W. S. Rodney, *Cauldrons in the Cosmos* (The University of Chicago Press, Chicago, 1988).
[2] W. Fowler, G. Caughlan, and B. Zimmerman, Annu. Rev. Astron. Astrophys. **13**, 69 (1975).
[3] C. A. Barnes, S. Trentalange, and S. C. Wu, Treatise on Heavy-ion Science, edited by D. A. Bromley, (Plenum, New York, 1985), Vol. 6, p. 3.
[4] L. R. Gasques, A. V. Afanasjev, E. F. Aguilera, M. Beard, L. C. Chamon, P. Ring, M. Wiescher, and D. G. Yakovlev, Phys. Rev. C **72**, 025806 (2005).
[5] E. M. Burbridge *et al*., Rev. Mod. Phys. **29**, 547 (1957).
[6] R. G. Stokstad *et al*., Phys. Rev. Lett. **37**, 888 (1976).
[7] L. J. Patterson *et al*., Astrophys. J. **157**, 367 (1969).
[8] M. Mazarakis *et al*., Phys. Rev. C **7**, 1280 (1973).
[9] M. D. High and B. Čujec, Nucl. Phys. **A282**, 181 (1977).
[10] J. R. Patterson *et al*., Nucl. Phys. **A165**, 545 (1971).
[11] B. Čujec and C. A. Barnes, Nucl. Phys. **A266**, 451 (1976).
[12] P. R. Christensen, Z. E. Switkowski, and R. A. Dayers, Nucl. Phys. **A280**, 189 (1977).
[13] H. Spinka *et al*., Nucl. Phys. **A233**, 456 (1974).
[14] G. Hulke *et al*., Z. Phys. A **297**, 161 (1980).
[15] S. C. Wu *et al*., Nucl. Phys. **A422**, 373 (1984); S. C. Wu, Ph.D. thesis, California Institute of Technology (1978).
[16] J. Thomas *et al*., Phys. Rev. C **31**, 1980 (1985).
[17] C. L. Jiang *et al*., Phys. Rev. Lett. **89**, 052701 (2002).
[18] C. L. Jiang, H. Esbensen, B. B. Back, R. V. F. Janssens, and K. E. Rehm, Phys. Rev. C **69**, 014604 (2004).
[19] C. L. Jiang *et al*., Phys. Rev. Lett. **93**, 012701 (2004).
[20] C. L. Jiang *et al*., Phys. Rev. C **71**, 044613 (2005).
[21] For the system $^{58}$Ni+$^{89}$Y, see C. L. Jiang *et al*., ANL Physics Division Annual Report ANL-05/61, p. 80.
[22] C. L. Jiang *et al*., Phys. Lett. **B640**, 18 (2006).
[23] C. L. Jiang, B. B. Back, H. Esbensen, R. V. F. Janssens, and K. E. Rehm, Phys. Rev. C **73**, 014613 (2006).
[24] C. Y. Wong, Phys. Rev. Lett. **31**, 766 (1973).
[25] K. Hagino, N. Takigawa, M. Dasgupta, D. J. Hinde, and J. R. Leigh, Phys. Rev. C **55**, 276 (1997).
[26] J. Fernández-Niello, C. H. Dasso, and S. Landowne, Comput. Phys. Commun. **54**, 409 (1989).
[27] D. D. Clayton, *Principles of stellar evolution and nucleosynthesis* (McGraw-Hill, New York, 1968).
[28] M. Beckerman, J. Ball, H. Enge, M. Salomaa, A. Sperduto, S. Gazes, A. DiRienzo, and J. D. Molitoris, Phys. Rev. C **23**, 1581 (1981).
[29] Ş. Mişicu and H. Esbensen, Phys. Rev. Lett. **96**, 112701 (2006).
[30] G. Michaud, Astrophys. J. **175**, 751 (1972); Phys. Rev. C **8**, 525 (1973).
[31] R. D. Evans, *The Atomic Nucleus* (McGraw-Hill, New York, 1955).
[32] G. Michaud, Phys. Rev. C **8**, 525 (1973).
[33] P. Rosales *et al*., Rev. Mex. Fís. **49** S4, 88 (2003).
[34] K. U. Kettner *et al*., Z. Phys. A **298**, 65 (1980).
[35] H. W. Becker *et al*., Phys. Rev. Lett. **38**, 337 (1977); Z. Phys. A **303**, 305 (1981).
[36] R. Dayras *et al*., Nucl. Phys. **A279**, 70 (1977).
[37] W. Galster *et al*., Phys. Rev. C **15**, 950 (1977).
[38] H. Voit *et al*., Phys. Lett. **B67**, 399 (1977).
[39] D. G. Kovar *et al*., Phys. Rev. C **20**, 1305 (1979).
[40] K. A. Erb, R. R. Betts, S. K. Korotky, M. M. Hindi, P. P. Tung, M. W. Sachs, S. J. Willett, and D. A. Bromley, Phys. Rev. C **22**, 507 (1980).
[41] W. Tren *et al*., Phys. Rev. C **22**, 2462 (1980).
[42] E. Eyal *et al*., Phys. Rev. C **13**, 1527 (1976).
[43] J. J. Kolata, R. C. Fuller, R. M. Freeman, F. Haas, B. Heusch, and A. Gallmann, Phys. Rev. C **16**, 891 (1977); J. J. Kolata, R. M. Freeman, F. Haas, B. Heusch, and A. Gallmann, *ibid*. **19**, 2237 (1979).
[44] I. Tserruya, Y. Eisen, D. Pelte, A. Gavron, H. Oeschler, D. Berndt, and H. L. Harney, Phys. Rev. C **18**, 1688 (1978).
[45] E. F. Aguilera *et al*., Phys. Rev. C **73**, 064601 (2006).
[46] H. J. Krappe, J. R. Nix, and A. J. Sierk, Phys. Rev. C **20**, 992 (1979).